2001 IEEE Aerospace Conference on the topic of "Missions, Systems, and Instruments for In Situ Sensing" (Session 2.05). March 10-17, 2001, Big Sky, Montana. http://aeroconf.org/.

Ultrasonic/Sonic Driller/Corer (USDC) as a Sampler for Future Planetary Exploration Missions

Yoseph Bar-Cohen, Stewart Sherrit, Benjamin P. Dolgin, Nathan Bridges, Xiaoqi Bao, Zensheu Chang, Ronald S. Saunders, JPL/Caltech, (MS 82-105), 4800 Oak Grove Drive,
Pasadena, CA 91109-8099, yosi@jpl.nasa.gov, web: http://ndeaa.jpl.nasa.gov
Dharmendra Pal, Jason Kroh, Tom Peterson
Cybersonics Inc., Erie, PA

Abstract – Future NASA exploration missions to Mars, Europa, Titan, comets and asteroids are seeking to perform sampling, in-situ analysis and possibly return of material to Earth for further tests. One of the major limitations of sampling in low gravity environments is the conventional drills need for high axial force. An ultrasonic/sonic driller/corer (USDC) mechanism was developed to address these and other limitations of existing drilling techniques. The USDC is based on an ultrasonic horn that is driven by a piezoelectric stack. The horn drives a free mass, which resonates, between the horn and drill stem. Tests have shown that this device addresses some of the key challenges to the NASA objective of planetary in-situ sampling and analysis. The USDC is lightweight (450 g), requires low preload (< 5N) and can be driven at low power (5W). The device has been shown to drill various rocks including granite, diorite, basalt and limestone. The drill can potential operate at high and low temperatures and does not require sharpening of the bit. Although the drill is driven electrically at 20 kHz, a substantial sub-harmonic acoustic component is found that is crucial to drilling performance. Models that explain this low frequency coupling in the horn, free mass, drill stem and rock is presented.

TABLE OF CONTENTS

1. INTRODUCTION

Performing efficient drilling and coring of rock materials has a great significance to NASA planetary program where a sample needs to be cored, in-situ analyzed and possibly returned to earth. Other fields that can also benefit from of an effective drilling including military, medical operations, construction, geology, sport (e.g., hiking), and games. Existing drilling techniques are limited by the need for large axial forces, high power consumption, and heavy mechanisms. Other areas of concern associated with conventional drillers is that they are subject to drill bit jamming, breaking, dulling and are difficult to use to perform non-horizontal or hard surfaces drilling. Also, the drilling process is hampered by the accumulation of drilling-debris in the drilled area. The life of coring bits is markedly reduced by the breakdown of the binder that holds the abrasive material on the bit surface. The ability of the new ultrasonic/sonic driller/corer to operate with minimum axial load (see Figure 1) is offering important enabling technology. Current research and development efforts of the authors are dedicated to understand the mechanism as well as analytically model its operation towards optimizing its performance.

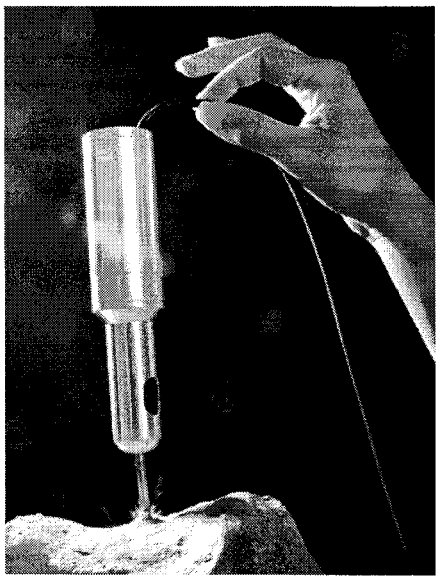

Figure 1 – A photographic view of the USDC held from its cable while coring sandstone. The minimal need for axial force is easily seen.

To establish the required analytical model a simultaneous theoretical and experimental studies have been launched and data were collected to assist in understanding the mechanism. The experimental setup consists of a USDC that is attached to test rig as shown in Figure 2 both schematically and

photographically. The device consists of three main parts; an ultrasonic actuator, a free mass and a drill stem. The analysis of the actuator circuit was based on the equivalent circuit of piezoelectric and acoustic elements as discussed by Mason [1 - 2] and was reported previously [3]. The horn was found to have a resonance at 21.5 kHz and the free tip velocity at resonance was determined to be linear with respect to the applied voltage and ranged from 1 to 10 m/s depending on the acoustic load.

The vibrations of the horn tip excite the free mass, which resonates between the horn tip and the top of the drill stem at frequency of the order of 1000 Hz. Acoustic energy in the free mass resonator is transferred to the top of the drill stem and propagates to the bit/rock interface where the rock is excited past its ultimate strain and fractures. In order to determine the critical issues related to the control and optimization of the drill, initial modeling of the acoustic interaction at the various interfaces of the drill are presented. The three interfaces that were studied are: 1) the interaction of the horn tip with the free mass, 2) the interaction of the free mass with the drill stem and 3) the interaction of the base of the drill stem (bit) with the rock.

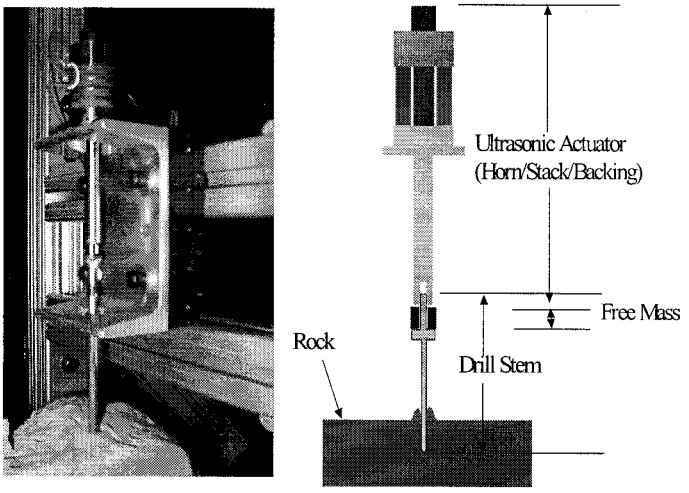

Figure 2 - Photograph and Schematic of the Ultrasonic/Sonic Driller/Corer

Generally, USDC is highly tolerant of changes in its operating environment. Because is it driven by piezoelectric ceramics, USDC can be designed to operate at a wide range of temperatures including those expected on Mars (-60C) and Venus (+450C). The coring bit creates a hole that is slightly larger than the drill bit diameter. This latter reduces the chances of bit jamming if the integrity of the hole is maintained, thus avoiding another problem associated with conventional drilling. The ultrasonic bit need not be sharp thus it does not have problems with bit dulling and wear. USDC is a novel device, not a conventional ultrasonic drill. Although the drill is driven electrically at 20 kHz a substantial sub-harmonic acoustic component is found that is crucial to drilling performance. An analytical model has been developed to explain this low frequency coupling in the horn, free mass behavior, drill stem, and rock interaction.

2. MODELING

In order to proceed with the modeling, the velocity/displacement of the horn tip during operation is required. Since the velocity/displacement depends on the acoustic load, a reasonable estimate of the velocity range can determined by calculating the horn tip velocity for the case where it is free and when the acoustic impedance is perfectly matched to produce maximum power in the acoustic load. The velocity of the tip as a function of the applied peak AC voltage is shown in Figure 3 for the two cases. The reasons for using the case where the acoustic load is ideal rather than clamped are twofold. Firstly, the acoustic power transferred to the rock is substantial which means that horn is well matched to the rest of the acoustic elements, and secondly, in order for the device to operate efficiently a gap must be present which means that for a substantial portion of the time the tip is not in contact with the free mass. For a peak AC voltage of 200 Volts on the drill the velocity is found to range between 1.25 m/s for the ideal load and 13.6 m/s for the free tip. The modeling of the interaction of the free mass can now be determined since the range of speeds of the horn tip have been set.

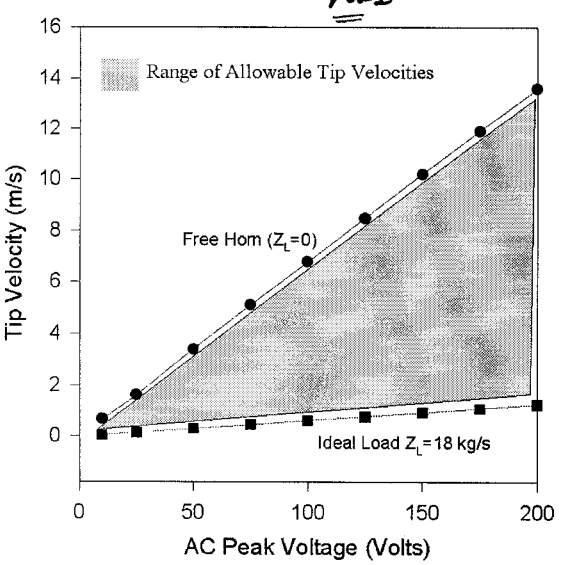

Figure 3 - The range of speed for the horn tip for an ideal load and for the unloaded horn.

Horn Tip – Free Mass Interaction

The free mass is driven by the horn tip, which vibrates at resonance frequency. A schematic of the model is

shown in Figure 4. The tip displacement is harmonic and is describe by

$$u = u_0\cos(\omega t + \theta). \quad (1)$$

The velocity of the horn tip is found by taking the time derivative of the displacement and is

$$v = -\omega u_0 \sin(\omega t + \theta). \quad (2)$$

Assuming the energy loss and time duration of the impact is negligible and the mass of the horn is much larger than

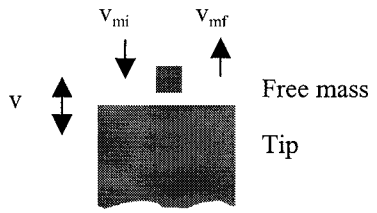

Figure 4 - A schematic of the free mass horn tip interaction model.

the free mass, we find using conservation of momentum and energy that

$$v_{mf} = v_{mi} + 2v \quad (3)$$

where v_{mi} is the free-mass velocity prior to interaction with horn and v_{mf} is the free mass velocity after interaction with the horn. A computer simulation model, which traces the positions of the free mass until it leaves the tip vibration range ($2u_0$) was written. The routine calculates the free mass speed after interaction with the horn. By keeping track of the free mass velocity the routine allowed us to explore this driving mechanism as a function of the horn position as the free mass crosses the plane of full extension (phase). The speed of the free mass as it leaves the interaction region versus position of the horn (position of tip represented as a phase angle t =0 at max displacement) is shown in Figure 5 for various ratios of v_{mi}/v.

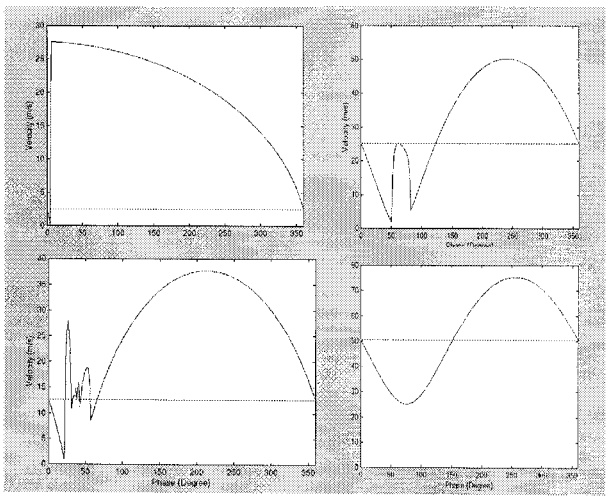

Figure 5 - The free mass velocity after interaction with the horn for v_{mi}=0.2,1,2,4v

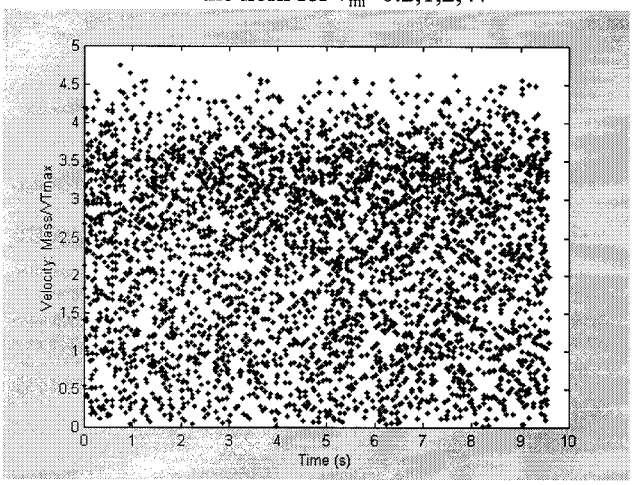

Figure 6 - The free mass velocity/maximum tip velocity as a function of time.

For all cases there is a net increase in the free mass velocity after interaction with the horn when averaged over phase. The computer model traces the movements of the free-mass and the horn. The movement of the horn is due to the reaction force on the horn tip and the force of gravity. In the calculation the free mass mass is set to 1 gram, the tip velocity amplitude is set to 1.26 m/s corresponding to displacement amplitude of 10 μm. The horn mass was 800 g. The energy loss of the free mass in each round trip is set as 75%. The simulation results shown in Figure 6 represent the ratio of the free mass velocity to the maximum horn tip velocity as a function of time. In addition the data was used to calculate the motion of the horn. The results show the random characteristics of the movement of the body of the horn. Figure 7 shows the horn tip position as a function of time. The motion is due to the impact interaction with the free mass.

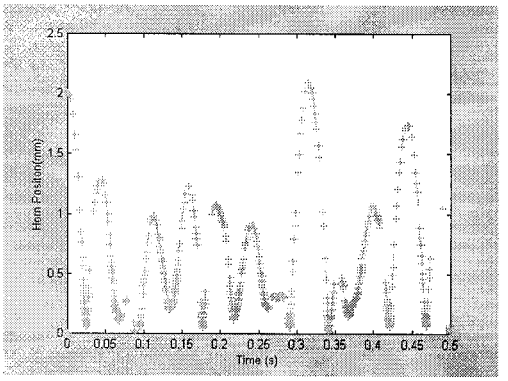

Figure 7 - The horn position as a function of time determined from model

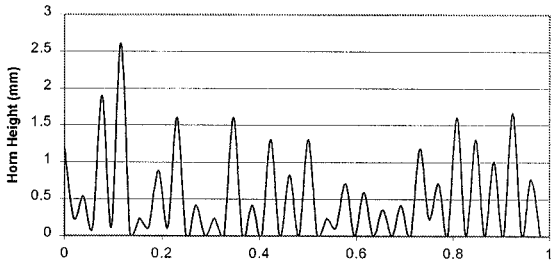

Figure 8 - The horn position as a function of time determined from high-speed camera.

The size, frequency and randomness of the jumps are confirmed by experimental observations shown in Figure 8 of the horn tip determined using a high-speed camera.

Free mass, Drill stem Interaction

The free mass impacts the top of the drill stem and creates a stress wave that propagates to the bit end. A finite element model was utilized to investigate the impact and resultant stress wave. Figure 9 shows results for the case where a cylindrical steel stem/bit of diameter 3.0 mm and length 100 mm with a concentric top cap of diameter 12 mm and length 6 mm. The impact used in the model is that of a free mass of 2 g with speed 1 m/s. The free mass has a curved surface at the contact area with a curvature of 10 mm. The free mass is assumed to be rigid and the bit end of the drill stem is clamped. Figure 9 shows the displacement of the surface of the free mass and the top surface of the drill stem during impact as a function of time. Figure 10 shows the resultant stress wave as a function of time at the bit end of the drill stem.

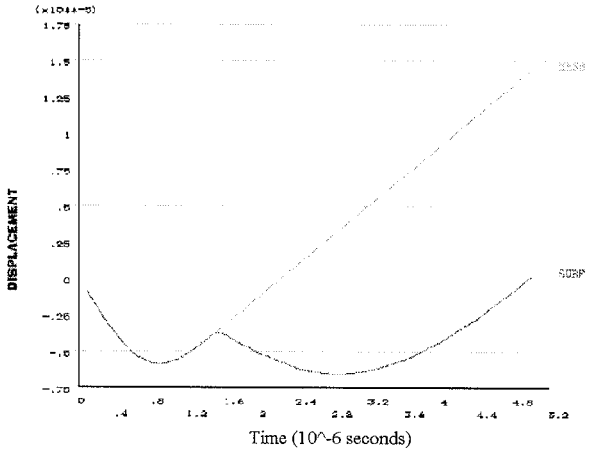

Figure 9 - The displacement as a function of time of the free mass and the top surface of the drill stem after impact.

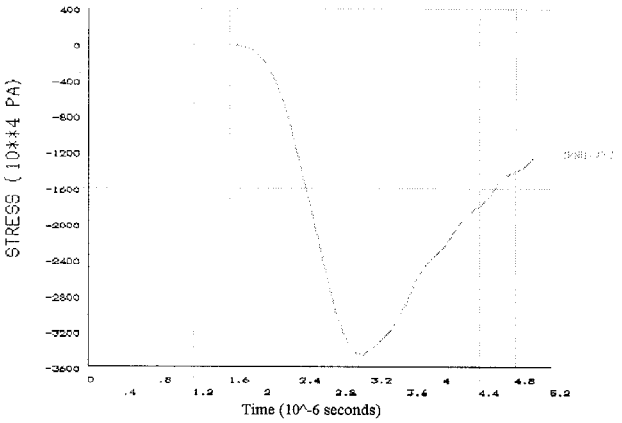

Figure 10 - The stress as a function of time of the free mass and the top surface of the drill stem after impact.

Bit Rock Interaction

In order to better understand the fracture of rocks under impact loading from a drill or a corer, a finite element model was developed using ANSYS. For the purpose of simplifying the problem, the rock is modeled as a circular cylinder with bottom surface fixed and the drill/corer impacts at the center of the top surface. This simplification makes the problem axis-symmetric. By using the axis-symmetric elements available in ANSYS, the original three-dimensional problem is now reduced to two-dimensions. The element size is made very fine near the drill/corer bit, and becomes coarser and coarser as it goes further away from the bit. Figure 11 shows a typical mesh for the problem outlined above.

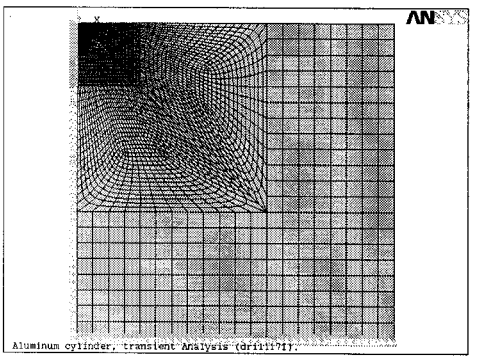

Figure 11- The mesh used to solve the bit rock interaction

Preliminary results were derived by assuming that the circular cylinder is made of isotropic material with a Young's modulus of 10 GPa and poisons ratio of 0.3. The impact loading from the drill has a peak value of .1 GPa and duration of 2.5 μsec, as shown in Figure 10.

Contour maps of the maximum principal strain were plotted and used as indication of fracture of rocks. It also shows how the elastic waves propagate in the rock. Figures 12 show the contour maps for the cylinder for drilling and coring, respectively. The drill bit is 3 mm in diameter. The corer has an inner diameter of 2 mm and an outer diameter of 3 mm.

The results show qualitative features of the rocks fracture under ultrasonic drilling or coring. From Figure 12 we find that the highest principal strain occurs at the edge of the drill bit. Also, the highest principal strain appears at both the outer and inner edge of the corer. It implies that the fracture is likely going to happen at the edge, which is confirmed by viewing the high speed filming during drilling. By comparing the various strain profiles in Figure 12, we find that the maximum principal strain under coring is higher than that under drilling, and the area of high principal strain under coring is also larger than that under drilling. It implies that with the same outer diameter and under the same loading, a corer will drill faster than a solid drill of the same diameter. This is confirmed by experiments.

The results have show how drilling and coring can be achieved with little or no preload. The next challenge is to integrate each of the models to determine the limits and optimization of the USDC.

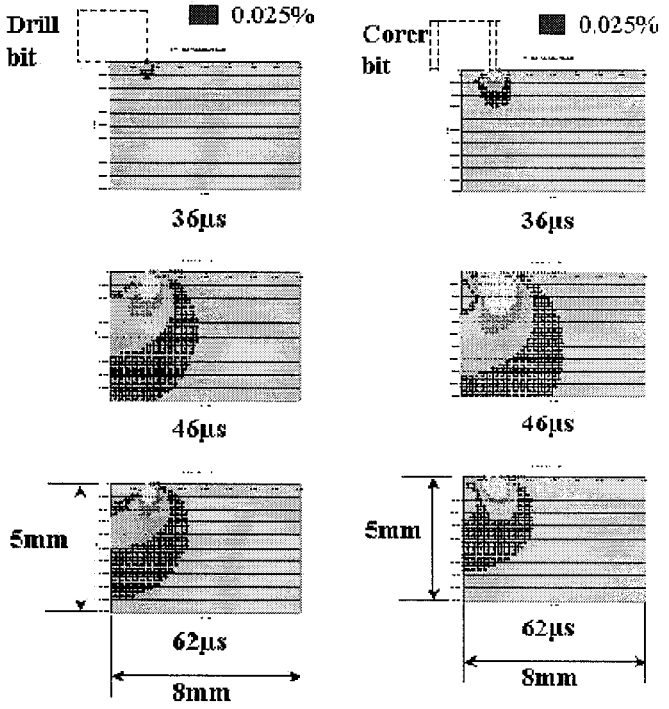

Figure 12 - The principle strain profile at various times after impact of the free mass on the drill stem for a drilling bit and a coring bit.

3. CONCLUSIONS

Models that explain the low frequency coupling of the USDC and the drilling under low axial preload have been presented. The results suggest a variety of avenues for optimization of the device. Current efforts are underway to integrate the various models to allow for the determination of system model with predictive and control abilities.

.

ACKNOWLEDGMENT

The authors would like to thank J.D. Carson for design and fabrication of the test apparatus. The research at the Jet Propulsion Laboratory (JPL), a division of the California Institute of Technology, was funded by the Mars Exploration Techogies under a contract with the National Aeronautics Space Agency (NASA).

REFERENCES

[1] W. P. Mason, Electromechanical Transducers and Wave Filters, Princeton, NJ, Van Nostrand, 1948

[2] W.P. Mason, Physical Acoustics and the Properties of Solids, D. Van Nostrand Co., Princeton, NJ, 1958

[3] S. Sherrit, B.P. Dolgin, Y. Bar-Cohen, D. Pal, J. Kroh, T. Peterson "Modeling of Horns for Sonic/Ultrasonic Applications," Proceedings of the IEEE International Ultrasonics Symposium, Lake Tahoe, CA, October 1999, pp. 647-651